

A Hyperspectral Anomaly Detection Algorithm Using Sub-Features Grouping and Binary Accumulation

Shurong Yuan^{ID}, Lei Shi^{ID}, Bo Yao^{ID}, Fangyan Li^{ID}, and Yuefan Du

Abstract—Most of the existing anomaly detection (AD) approaches for hyperspectral images (HSIs) usually achieve high detection accuracy at the cost of high computational complexity. To meet the needs of actual detection scenarios (efficiency, robustness, and accuracy), this letter introduces a fast and robust AD algorithm via subfeatures grouping and binary accumulation (SFBA) for HSIs. We propose a spatial-spectral anomaly scoring strategy to improve detection accuracy. A number of spectral subfeatures of HSI are selected and divided into N groups as the detection input information and the proposed scoring strategy is carried out for N group data, respectively, to improve the detection efficiency. Then binary accumulation is introduced to improve the robustness of AD algorithm by accumulating detection results of each group. Our proposed detection algorithm was compared with the existing algorithms on real hyperspectral datasets, thereby verifying its strong robustness and low computational complexity simultaneously.

Index Terms—Anomaly detection (AD), binary accumulation, histogram, hyperspectral image (HSI), subfeatures grouping.

I. INTRODUCTION

HYPERSPECTRAL image (HSI) is a 3-dimensional data cube [1]. Each pixel in HSI is considered as a high-dimensional vector, which provides more rich characteristic information of target objects [2], [3]. Anomaly detection (AD) for HSI, simply using spectral and spatial anomaly characteristics to detect anomalous targets and requiring no prior information of target and background, have attracted much attention worldwide. With respect to the spectral anomaly characteristics, the spectrum of anomaly target in hyperspectral remote sensing distinguishes significantly from the surrounding background [4], [5], [7]. In regard to the spatial anomaly characteristics, anomaly target is usually small, exhibiting its sparse distribution in HSIs [8].

In the past few decades, lots of different kinds of AD methods for HSIs have been developed by researchers. The well-known Reed-Xiaoli detector (RXD) [9] assumed that the

Manuscript received September 26, 2021; revised December 2, 2021, January 22, 2022, and February 21, 2022; accepted February 28, 2022. Date of publication March 2, 2022; date of current version March 21, 2022. This work was supported in part by the National Natural Science Foundation of China under Grant 61871302, Grant 62101406, and Grant 62001340; and in part by the Fundamental Research Funds for the Central Universities under Grant JB211311. (*Shurong Yuan and Lei Shi are co-first authors.*) (*Corresponding author: Lei Shi.*)

The authors are with the School of Aerospace Science and Technology, Xidian University, Xi'an 710071, China (e-mail: sryuan@stu.xidian.edu.cn; shilei2002yoda@163.com; yaob@xidian.edu.cn; fyl@xidian.edu.cn; yuefandu@stu.xidian.edu.cn).

Digital Object Identifier 10.1109/LGRS.2022.3156057

spectral characteristics of HSI background follows Gaussian distribution, which is too strict to be satisfied in reality. Later, some modified RX algorithms were proposed [10], [11] to alleviate the strict constraints of distribution, such as weighted-RX, kernel-RX, and so on. However, the RX-based algorithms only use the characteristics of spectral anomaly and a fixed distribution model that cannot satisfy all the background information of HSI, resulting in weak robustness and low detection accuracy. To avoid the inherent deficiency of the inappropriate model of data distribution in RX, many other algorithms were also proposed [12]–[14]. The selection-based discriminative forest algorithm (SSDF) used the spatial anomaly characteristics of HSI [15], which exhibited low complexity but poor robustness. Ma *et al.* [16] proposed a new anomaly detector Integration of Feature Extraction and Background Purification (FEBPAD) based on low rank and sparse matrix decomposition Low-rank and sparse representation (LRASR) algorithm [17] separates the anomaly and the background parts, in which the background is assumed to occur in the lowest-rank representation of the image. By assuming low-rank background and sparse anomaly, Huyan *et al.* [18] proposed PAB-dc that decomposes HSIs into three types as background, anomaly, and noise to realize better performance of AD. However, its performance is highly correlated with the dictionary used. If the background dictionary is contaminated by anomalies, it may result in low detection rate. From the above, despite that the detection accuracy of representation-based algorithms has been greatly improved, these algorithms need construct online dictionary, thereby complicating themselves. In addition, most of the AD algorithms cannot fully utilize the spectral and spatial characteristics of anomaly target, thereby deteriorating their detection accuracy and robustness.

In this letter, we propose a fast and robust AD algorithm based on subfeatures grouping and binary accumulation (SFBA) for HSIs. The novelties and key contributions are formulated as follows: 1) the axis-parallel subspace selection [19], exhibiting low computational complexity, is applied to HSIs to reduce the band redundancy of HSIs and improve detection efficiency; 2) compared with the traditional AD algorithm that only uses the spectral difference between the anomaly targets and the background, we propose a spatial-spectral anomaly scoring strategy, which not only utilizes the spectral difference but also fully utilizes the spatial sparsity of anomalous targets. More prior information is provided in AD, thus improving the detection accuracy of the AD algorithm;

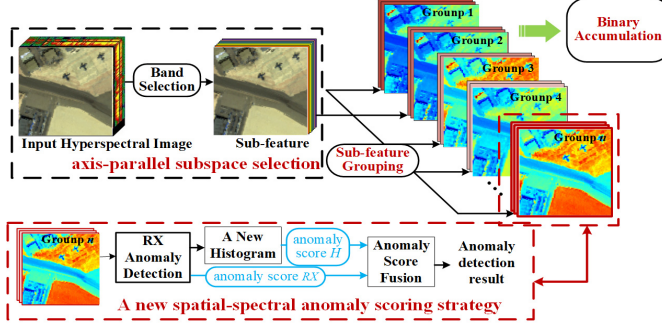


Fig. 1. Flowchart of the proposed SFBA algorithm for AD of HSIs.

and 3) based on the guidance that false detection pixels appear at random positions and anomaly targets appear at a fixed position in each group, a binary accumulation process is proposed to improve the algorithm's robustness. In summary, our proposal can reduce the complexity of AD algorithm while ensuring strong robustness and high detection accuracy. The robustness and detection efficiency of the proposal is verified by analyzing different databases and algorithm complexity, respectively. The detection accuracy of the proposed AD algorithm is further verified through ROC curve and value of AUC. In view of the limited computing resources on the space-based satellite and the complicated background of the observation, the proposed AD algorithm can potentially be applied to the real-time anomaly targets online monitoring.

II. FAST AND ROBUST AD

The basic procedure of the proposed SFBA algorithm is illustrated in Fig. 1. The SFBA AD algorithm is composed of four parts: band selection, subspace grouping, anomaly scoring stage, and binary accumulation. The detailed description is presented in the following subsections. Subsection II-A introduces the band selection algorithm for AD. Subsection II-B highlights a novel low-complexity anomaly scoring strategy based on spectral and spatial anomalies of HSIs. Subsection II-C explains the binary accumulation.

A. Axis-Parallel Subspace Selection Method

When the number of samples is constant, the performance of the AD algorithm that uses full-dimensional features cannot achieve the expected results. Aggarwal [20] has verified that the distance-based methods fail to differentiate from the normal instances because objects are almost all equidistant in high-dimensional space. These challenges can be overcome by extracting sub-features that are beneficial for AD and neglecting other redundant bands. The axis-parallel subspace method has proven to be an effective feature selection method that can reduce these irrelevant attributes due to its simple principle and the abilities of retaining the information of anomalous targets [20].

In fact, the principle of the axis-parallel subspace method lies in selecting a subset of bands according to the variance of each subfeatures. The band with small variance value is selected as the subfeatures, which is opposite to the nature of principal component analysis (PCA).

Let hyperspectral data be noted as $Y \in R^{h \times \omega \times d}$, where d is the number of the spectral bands, h and ω are the 2-D

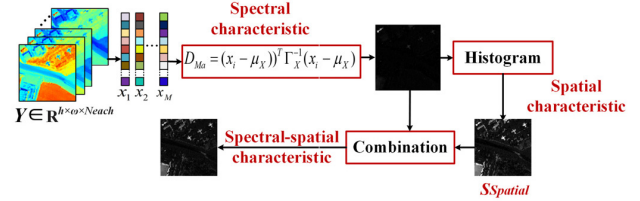


Fig. 2. Flowchart of the proposed anomaly scoring strategy.

image sizes in a fixed band of the data. For ease of calculation, the 3-D cube Y is transformed into a 2-D matrix $X = [x_1, x_2, \dots, x_M]$, where $x_i \in R^d$ and $M = h \times \omega$. The projection of x_i onto the j th band is denoted by x_{ij} . Then the variance of j th band can be expressed as

$$\text{var}_j = \frac{\sum_{i=1}^M (\text{dist}(x_{ij}, u_j))^2}{\text{Card}(X)} \quad (1)$$

where $\text{Card}(X)$ is the cardinality of X , u_j is the mean value of all pixels in the j th band, dist is the Euclidean distance between x_{ij} and u_j . The method of axis-parallel subspace selection chooses those bands with a smaller var_j as the input data for the proposed SFBA model. The subfeature numbers can be expressed as N_{sub} . Then the N_{sub} bands are randomly divided into n groups as shown in Fig. 1. The band numbers of each group have the same value N_{each} . The influence of N_{each} of SFBA will be discussed in Section III.

B. Novel Spatial–Spectral Anomaly Scoring Strategy

In this subsection, we present a novel anomaly scoring strategy that takes into account the characteristics of spatial and spectral anomalies of HSIs. This strategy can improve the accuracy of anomaly scoring of HSIs without increasing the computational complexity of the algorithm. The flowchart of the anomaly scoring strategy is shown in Fig. 2, and the anomaly score of each subfeature group in Fig. 1 is annotated with the proposed spatial–spectral anomaly scoring strategy. According to the characteristics of the anomalies in HSIs, the spectral anomaly can be regarded as anomalies with different spectra form the background. The spatial anomaly considers that anomalous targets are often sparsely distributed in HSIs with a low occurrence probability. For spectral detection, it is simple and efficient to implement Mahalanobis distance on each subfeature group. The spectral detection result can be described as follows:

$$D_{Ma} = (x_i - \mu_X)^T \Gamma_X^{-1} (x_i - \mu_X), \quad i = 1, \dots, M \quad (2)$$

where $x_i \in R^{N_{\text{each}} \times 1}$ is the i th pixel in the selected subfeature group with N_{each} bands, $\mu_X \in R^{N_{\text{each}} \times 1}$ and $\Gamma_X \in R^{N_{\text{each}} \times N_{\text{each}}}$ are the mean vector and covariance matrix of X . Reed and Yu [9] pointed out that larger Mahalanobis distance implies more anomalous pixels. Furthermore, it can be seen from (2) that the main computational cost for implementing Mahalanobis distance is to solve the inverse of the covariance matrix Γ_X . The computational complexity of N_{each} -order matrix inversion can be expressed as $O(N_{\text{each}}^3)$, thereby greatly reducing the computational complexity of N_{each} -order matrix inversion can be computational complexity compared to AD on full bands.

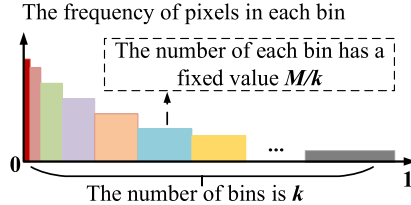


Fig. 3. Frequency of pixels falling into each bin.

The spatial characteristics of anomalous targets can be represented as sparse distribution of anomalous targets in the entire HSIs. Then, for anomaly targets, their corresponding values in D_{Ma} are similar and have a sparse distribution. The histogram based on D_{Ma} can just indicate the distribution frequency of anomaly scores, which can be used to indicate the sparsity of each pixel. The lower the height of the bin in histogram, and the more likely the corresponding anomalous targets are. Therefore, to take advantage of the sparsity of anomalous targets in space, our proposed novel spatial-spectral anomaly scoring strategy introduces a histogram of D_{Ma} to represent the sparsity of each pixel. Introducing the calculation of the histogram of D_{Ma} hardly increase the computational complexity of the AD, but effectively utilizes the sparsity of anomalous targets. Fig. 3 shows a kind of dynamic bin-width histograms that is determined as Table I.

The bin in Fig. 3 covering a larger interval of the value range has less height, suggesting that the pixels in the bin are sparsely distributed. Taking full advantage of the sparsity of the anomaly targets, we argue that larger horizontal axis span of histogram indicates higher possibility of confirming anomaly targets. The spatial anomaly score of the pixels corresponding to the k th bin are expressed as

$$S_{\text{spatial}}(k) = \log\left(\frac{1}{\text{hist}(k)}\right) \quad (3)$$

where $\text{hist}(k)$ is the value of height of each bin. The final anomaly scoring S_{total} , combining D_{Ma} and S_{spatial} according to the importance of anomaly information they contain, is a spatial-spectral anomaly scoring strategy and is shown as follows:

$$S_{\text{total}} = \frac{\lambda_D}{\lambda_S + \lambda_D} D_{Ma} + \frac{\lambda_S}{\lambda_S + \lambda_D} S_{\text{spatial}} \quad (4)$$

where λ_S and λ_D are the larger eigenvalues of the tensor matrix from D_{Ma} and S_{spatial} . The eigenvalue often corresponds to the important information implicit in the matrix, whose importance positively correlates with its magnitude. Thus, λ_S and λ_D represent the anomaly information of HSI. If the larger the value of λ_D is, the more anomaly information in D_{Ma} is contained, and the larger the proportion of D_{Ma} in the fusion process.

C. Binary Accumulation

To improve the robustness and detection accuracy of AD for HSIs, this subsection proposes a binary accumulation method. HSI, a 3-dimensional data cube, provides a wealth of spectral information to uniquely identify various materials by their reflective spectrum with a uniform spatial distribution.

TABLE I

ALGORITHM OF SPATIAL ANOMALY SCORE

Input: the spectral detection result D_{Ma} , the number of values in D_{Ma} M , the number of bins k ,
Output: the spatial detection result S_{spatial}
1 Convert 2-D D_{Ma} into 1-D array D_{Ma_1} ;
2 Sort D_{Ma_1} : $\text{sort}_D D_{Ma}$;
3 Divide $\text{sort}_D D_{Ma}$ into k bins: $bin_1, bin_2, bin_3 \dots bin_k$ (each bin has a fixed number of pixel M/k);
4 Calculate the width of bin_i : $width_i = last_val_i - first_val_i$ ($last_value_i$ is the last value of bin_i ; $first_value_i$ is the first value of bin_i);
5 Calculate the height of bin_i : $hist(k) = M / (k * width_i)$;
6 Calculate the spatial anomaly result of k -th bin: $S_{\text{spatial}}(k) = \log(1/hist(k))$.

The proposed algorithm presupposes that the real anomaly target locations are fixed in detection result map of each group, and that the detected false anomaly target location in each group is random. Under this hypothesis, each time a group detection result is accumulated during the process of binary accumulation. Therefore, the real positions of anomaly target have the highest energy after conducting binary accumulation.

The result map $M_{\text{total}}(i, j, n)$ of spectral-spatial AD is defined according to the following equation:

$$M_{\text{total}}(i, j, n) = \begin{cases} 0, & \text{if } S_{\text{total}}(i, j, n) < \text{Val}_{\text{threshold}} \\ 1, & \text{if } S_{\text{total}}(i, j, n) > \text{Val}_{\text{threshold}} \end{cases} \quad (5)$$

where i, j is the position coordinates, n represents the n th group after subspace grouping, $\text{Val}_{\text{threshold}}$ is the detection threshold, and $S_{\text{total}}(i, j, n)$ is the value of spatial-spectral anomaly scoring in n th group. When the value of anomaly score is greater than $\text{Val}_{\text{threshold}}$, the pixel is considered to be an anomaly target, otherwise a background. Based on the N groups of spectral-spatial AD map, a binary accumulation matrix $B(i, j)$ is established as follows:

$$B(i, j) = \sum_{n=1}^N M_{\text{total}}(i, j, n). \quad (6)$$

In this letter, the position corresponding to the large energy accumulation value in binary accumulation result is regarded as the position of the anomaly target.

III. EXPERIMENT AND ANALYSIS

To illustrate the performance of the SFBA algorithm, six state-of-the-art algorithms are selected to make comparisons in this section in terms of algorithm complexity and detection accuracy. They involve GRX [9], GLRT [10], SSDF [15], FEBPAD [16], LRASR [17], and PAB-dc [18].

A. Hyperspectral Datasets

As shown in Fig. 4, three HSI datasets are chosen to show the performance of the proposed SFBA. The first data source is obtained by the Reflective Optics System Imaging Spectrometer sensor [21]. This dataset describes a scene of Pavia city center. The second and third data source originates from an open Airport-Beach-Urban dataset [22]. The sample images in this dataset were manually extracted from large images downloaded from the AVIRIS website.

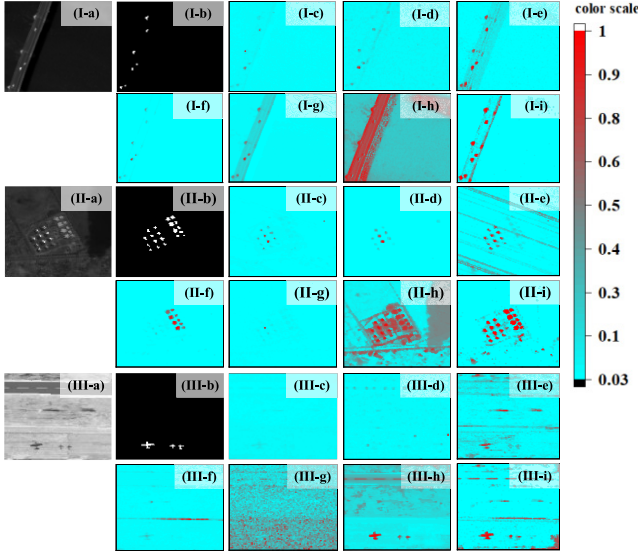


Fig. 4. Detection maps of different algorithms. (I) Pavia City dataset. (II) Texas Coast dataset. (III) Gulfport dataset. (a) Subimage. (b) Reference map. (c) Global RX. (d) GLRT. (e) SSDF. (f) FEBPAD. (g) LRASR. (h) PAB-DC. (i) SFBA.

B. Experimental Result and Discussion

The receiver operating characteristic (ROC) curve is a kind of popular performance assessment criterion for target detection applications and the integration of ROC curve is defined as the area under the curve (AUC). Hence, the ROC and AUC curves are used to conduct fair analysis and comparison with respect to the performance of the AD algorithm in this letter.

For the purpose of verifying the robustness of our proposed algorithm, we analyzed the proposed algorithm on three datasets with increasing background complexity: Pavia City dataset, Texas Coast dataset, and Gulfport dataset. The Pavia City data source and the Texas Coast data source have a relatively simple background, in which large difference exists between the anomaly targets and the background. In contrast, the background in the data sources of Gulfport dataset is more complicated. The following shows the analysis results of the proposed algorithm on these three datasets. The parameters of the SFBA algorithm are set to fixed values as follows. $N_{\text{sub}} = 40$, $n = 8$, $N_{\text{each}} = 5$, $\text{Val}_{\text{threshold}} = 0.4$, $k = 2h$, where N_{sub} is the number of the selected subfeature, n is the number of groups, N_{each} is the number of bands in each group, $\text{Val}_{\text{threshold}}$ is the detection threshold in the result map of spectral–spatial AD, k is the number of bins, and h is the height of the HSI. The color detection maps using three datasets are shown in Fig. 4.

The ROC curves are presented in Fig. 5, and the AUC values are demonstrated in Table II. For random grouping of SFBA, the AUC is different under each experiment. The AVE, max, min, and STD in Table II is the average, maximum, minimum, and standard deviation of AUC of proposal with 100× repeated experiments. It shows that the maximum of AUC of the proposed SFBA can achieve the best detection effect in the dataset with simple background, such as in Pavia City. Even Gulfport dataset and Texas Coast datasets, which have complex backgrounds, the average value of AUC value

TABLE II
AVERAGE AUC VALUE OF ROC CURVE ON ALL DATASETS

AUC	Pavia City	Texas Coast	Gulfport
Global RX	0.9982	0.9946	0.9526
GLRT	0.9982	0.9946	0.8456
SSDF	0.9962	0.8976	0.9456
FEBPAD	0.9946	0.9913	0.9353
LRASR	0.9995	0.9953	0.4681
PAB-DC	0.9019	0.9924	0.9497
SFBA	$AVE_{\text{min}}^{+0.0049}$ $0.9948^{+0.0049}_{-0.0043}$	$0.9981^{+0.0011}_{-0.0009}$	$0.9650^{+0.0153}_{-0.0428}$
<i>STD</i>	0.0012	0.0004	0.0106

TABLE III
DETECTION TIME OF AD ON ALL DATASETS

Time	Pavia City	Texas Coast	Gulfport
Global RX	0.19925	0.28938	0.31089
GLRT	14.783	43.489	34.3606
SSDF	66.865	48.630	61.3546
FEBPAD	2.8846	4.4643	4.22815
LRASR	286.88	355.58	200.677
PAB-DC	1619.1	979.81	501.897
SFBA	0.39223	0.33664	0.5126

of the proposed SFBA shows the best-performing detection algorithm. It can be proved that the algorithm is robust and applied to a wide range of scenarios.

Table III shows the speed of AD algorithm in MATLAB under the same computing environment. It can be seen that hardly can any of those algorithms realize real-time detection due to high computational complexity of the existing high-accuracy detection algorithms. Despite Global RX exhibiting a shorter operation time, its low detection accuracy must not be neglected. The computational complexity of Global RX can be expressed as $O(d^3) + O(d^2)$. However, when our proposed AD algorithm that is based on subfeatures grouping operates in parallel on hardware, the computational complexity is only $O(N_{\text{each}}^3) + O(N_{\text{each}}^2) + O(2nM)$. In this expression, d is the number of spectral bands in HSI, N_{each} is the number of subfeatures of each group of HSIs after grouping, n is the number of groups, and M is the number of pixels in HSIs. Usually, the number of bands d in the HSIs can reach several hundreds, whereas N_{each} of the SFBA algorithm is greatly reduced compared to d . Therefore, the proposed SFBA can realize fast anomaly target detection.

C. Parameter Analysis

The influence of the value of subfeatures N_{sub} , groups n , bins in histogram k on the performance of the SFBA is analyzed in Fig. 6. Fig. 6(a) shows the variation of AUC of the dataset, when the value of N_{sub} changes from 10 up to 100 and $n = 8$. It can be observed that when performing AD on Pavia City and Texas Coast datasets that are characterized with simple backgrounds, only a small number of subfeatures can be selected to obtain higher detection accuracy. However, for HSIs with complex backgrounds (i.e., Gulfport dataset), more subfeatures are required to achieve high detection accuracy. When the number of subfeatures exceeds 40, the AUC tends to be stable with strong robustness. Fig. 6(b) illustrates the value of the AUC analysis effect of n on the performance of the proposed algorithm. The other parameters are fixed as

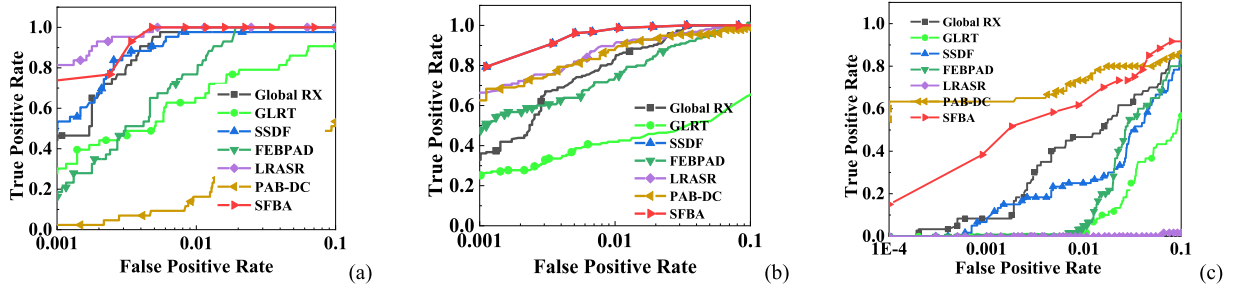


Fig. 5. ROC curves of different methods. (a) Pavia City dataset. (b) Texas Coast dataset. (c) Gulfport dataset.

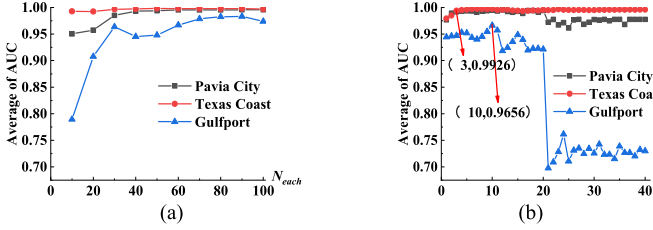


Fig. 6. Impact of the parameters. (a) Subfeatures N_{sub} . (b) Groups n .

$N_{\text{sub}} = 40$, $\text{Val}_{\text{threshold}} = 0.4$, and $k = 2h$. The total number of the selected subfeature N_{sub} is a fixed value, which results in a larger number of groups corresponding to less spectral bands in each group. From the perspective of the proposed SFBA, a large number of groups is beneficial to the binary accumulation process, whereas the smaller number of spectrum bands included in each group degrades the performance of the spectral detection result D_{Ma} . Result shows that when the value of n ranges between 3 and 10, the proposed SFBA exhibits strong robustness even in Gulfport dataset that are characterized with complex backgrounds.

IV. CONCLUSION

In this letter, we propose an ingenious hyperspectral AD algorithm via using SFBA to realize fast and robust AD. Experiments using different HSI datasets have verified that the AUC values of our proposal with fixed parameters are no less than 0.97 with the detection time of less than 0.5 s, outperforming the other state-of-the-art AD methods. The experimental results have validated that our proposed SFBA is robust and fast, which can be applied in real-time AD applications for HSIs.

ACKNOWLEDGMENT

The authors would like to thank the handling editor and the anonymous reviewers for their critical and constructive review of the manuscript.

REFERENCES

- [1] L. Zhang, M. Lan, J. Zhang, and D. Tao, "Stagewise unsupervised domain adaptation with adversarial self-training for road segmentation of remote-sensing images," *IEEE Trans. Geosci. Remote Sens.*, vol. 60, pp. 1–13, 2022.
- [2] F. Luo, Z. Zou, J. Liu, and Z. Lin, "Dimensionality reduction and classification of hyperspectral image via multistructure unified discriminative embedding," *IEEE Trans. Geosci. Remote Sens.*, vol. 60, pp. 1–16, 2022.
- [3] F. Luo, H. Huang, Z. Ma, and J. Liu, "Semisupervised sparse manifold discriminative analysis for feature extraction of hyperspectral images," *IEEE Trans. Geosci. Remote Sens.*, vol. 54, no. 10, pp. 6197–6211, Oct. 2016.
- [4] J. Hu, Y. Zhang, M. Zhao, and P. Li, "Spatial-spectral extraction for hyperspectral anomaly detection," *IEEE Geosci. Remote Sens. Lett.*, vol. 19, pp. 1–5, 2022.
- [5] X. Shang, M. Song, Y. Wang, and H. Yu, "Residual-driven band selection for hyperspectral anomaly detection," *IEEE Geosci. Remote Sens. Lett.*, vol. 19, pp. 1–5, 2022.
- [6] B. Du and L. Zhang, "A discriminative metric learning based anomaly detection method," *IEEE Trans. Geosci. Remote Sens.*, vol. 52, no. 11, pp. 6844–6857, Nov. 2014.
- [7] A. Taghipour and H. Ghassemian, "Hyperspectral anomaly detection using attribute profiles," *IEEE Geosci. Remote Sens. Lett.*, vol. 14, no. 7, pp. 1136–1140, Jul. 2017.
- [8] B. Sun, X. Kang, S. Li, and J. A. Benediktsson, "Random-Walker-based collaborative learning for hyperspectral image classification," *IEEE Trans. Geosci. Remote Sens.*, vol. 55, no. 1, pp. 212–222, Jan. 2017.
- [9] I. S. Reed and X. Yu, "Adaptive multiple-band CFAR detection of an optical pattern with unknown spectral distribution," *IEEE Trans. Acoust., Speech, Signal Process.*, vol. 38, no. 10, pp. 1760–1770, Oct. 1990.
- [10] J. Liu, Z. Hou, W. Li, R. Tao, D. Orlando, and H. Li, "Multipixel anomaly detection with unknown patterns for hyperspectral imagery," *IEEE Trans. Neural Netw. Learn. Syst.*, early access, Apr. 14, 2021, doi: [10.1109/TNNLS.2021.3071026](https://doi.org/10.1109/TNNLS.2021.3071026).
- [11] H. Kwon and N. M. Nasrabadi, "Kernel RX-algorithm: A nonlinear anomaly detector for hyperspectral imagery," *IEEE Trans. Geosci. Remote Sens.*, vol. 43, no. 2, pp. 388–397, Feb. 2005.
- [12] S. Matteoli, M. Diani, and G. Corsini, "Hyperspectral anomaly detection with kurtosis-driven local covariance matrix corruption mitigation," *IEEE Geosci. Remote Sens. Lett.*, vol. 8, no. 3, pp. 532–536, May 2011.
- [13] J. E. Fowler and Q. Du, "Anomaly detection and reconstruction from random projections," *IEEE Trans. Image Process.*, vol. 21, no. 1, pp. 184–195, Jan. 2012.
- [14] Y. Gu, Y. Liu, and Y. Zhang, "A selective KPCA Algorithm based on high-order statistics for anomaly detection in hyperspectral imagery," *IEEE Geosci. Remote Sens. Lett.*, vol. 5, no. 1, pp. 43–47, Jan. 2008.
- [15] S. Chang, B. Du, and L. Zhang, "A subspace selection-based discriminative forest method for hyperspectral anomaly detection," *IEEE Trans. Geosci. Remote Sens.*, vol. 58, no. 6, pp. 4033–4046, Jun. 2020.
- [16] Y. Ma, G. Fan, Q. Jin, J. Huang, X. Mei, and J. Ma, "Hyperspectral anomaly detection via integration of feature extraction and background purification," *IEEE Geosci. Remote Sens. Lett.*, vol. 18, no. 8, pp. 1436–1440, Aug. 2021.
- [17] Y. Xu, Z. Wu, J. Li, A. Plaza, and Z. Wei, "Anomaly detection in hyperspectral images based on low-rank and sparse representation," *IEEE Trans. Geosci. Remote Sens.*, vol. 54, no. 4, pp. 1990–2000, Mar. 2016.
- [18] N. Huyan, X. Zhang, H. Zhou, and L. Jiao, "Hyperspectral anomaly detection via background and potential anomaly dictionaries construction," *IEEE Trans. Geosci. Remote Sens.*, vol. 57, no. 4, pp. 2263–2276, Apr. 2019.
- [19] H.-P. Kriegel, P. Kröger, E. Schubert, and A. Zimek, "Outlier detection in axis-parallel subspaces of high dimensional data," in *Proc. Pacific-Asia Conf. Knowl. Discovery Data Mining*, 2009, pp. 831–838.
- [20] C. C. Aggarwal, *High-Dimensional Outlier Detection: The Subspace Method*. Cham, Switzerland: Springer, 2013, pp. 135–167.
- [21] Y. Zhang, B. Du, L. Zhang, and S. Wang, "A low-rank and sparse matrix decomposition-based Mahalanobis distance method for hyperspectral anomaly detection," *IEEE Trans. Geosci. Remote Sens.*, vol. 54, no. 3, pp. 1376–1389, Mar. 2016.
- [22] X. Kang, X. Zhang, S. Li, K. Li, J. Li, and J. A. Benediktsson, "Hyperspectral anomaly detection with attribute and edge-preserving filters," *IEEE Trans. Geosci. Remote Sens.*, vol. 55, no. 10, pp. 5600–5611, Oct. 2017.